Effect of W on the evolution of precipitates in Ni-Co-Cr-W-Mo super-alloys

Han-sheng BAO[1], Zhi-hua GONG[1,2], Zheng-zong CHEN[1], Gang YANG[1], Zheng-dong LIU[1]

1. Institute for Special Steels, Central Iron and Steel Research Institute, Beijing 100081, China;

2. Inner Mongolia University of Science & Technology, Baotou 014010 China.

*Corresponding author: Han-sheng BAO, professor; E-mail:Baohansheng@nercast.com.

*Co- corresponding author: Zhi-hua GONG, Vice professor; E-mail:gzh_2001@163.com.

Abstract: The Ni-Co-Cr-W-Mo system is critical for the design of nickel-based super-alloys. This system stabilizes different topologically close packed (TCP) phases in many of the commercially super-alloys with high W and Mo contents. Scanning electron microscopy (SEM), transmission electron microscopy (TEM), and thermodynamic calculations are applied to investigate the thermodynamics of the precipitates in two different W content Ni-Co-Cr-W-Mo super-alloys. Computational thermodynamics verified experimental observation of the f u phase formation as a function of temperature and alloy chemistry, but the kinetics for the precipitation of M_6C phase do not agree with the experimental findings. The major precipitates of alloy 1 at temperatures 700 and 750 °C during long time exposure are $M_{23}C_6$, γ′ phase, and MC, and alloy 2 are $M_{23}C_6$, γ′ phase, MC, M_6C and u phase. The W addition is found to promote the precipitation of M_6C and u phase during exposure. The M_6C has higher W and lower Ni content than that of u phase, meanwhile, M_6C is an unstable phase would transform into $M_{12}C$ after 5000 h exposure at 750 °C. A great quantity of needle-like u phases precipitated after exposure at 750 °C for 5000h, which have no effect on the impact property of alloy 2.

Key words: nickel-based super-alloys; M_6C; u phase; long time exposure; $M_{12}C$;

1. Introduction

As the development of advanced ultra-supercritical coal-fired power plants, the steam presure will reach 35 MPa, the steam temperature will be over 700 °C, and the thermal efficiency will be over 50% in the future [1-3]. Fe-based heat resistant steels, like the steels for main steam pipe, re-heater (or super-heater) tube and blade, etc, can not meet the manufacturing requirements of key high temperature components, when the steam temperature of power station is over 650 °C[4-5]. Thus, some Nickel-based alloys such as Waspaloy, USC 141, ACC 617 and Inconel 718 are candidates for turbines and pipes [6-7].

Tungsten (W), whose atomic radius is larger than that of Mo, can produce larger lattice distortion. So the solution strengthening in the alloys with W is stronger. Meanwhile, the addition of W will be conducive to improve the creep fracture strength of the alloy， because it can reduce the stacking fault energy[8].Therefore, W has been added to replace part of molybdenum (Mo) in some heat-resistant steel, such as the TOS110 and HR1200 heat resistant steels [9], for improving the high temperature creep fracture life. In addition, W is also widely used in nickel-based single

crystal alloys to improve the service temperature [10].

Waspaloy is a nickel-based super-alloy strengthened by nanometer-size γ′ phase and $M_{23}C_6$ carbide. W can improve the stability of γ′ phase through changing the distribution of alloy elements in γ′-γ matrix. Thus, some W element is added to replace part Mo of Waspaloy nickel-based super-alloy. And a newly wrought Nickel-based super-alloy used for steam turbine blades was exploited based on Waspaloy by our group recently. While excess refractory elements such as W and Mo add to the alloy will promote the formation of a phase family known as topologically close packed (TCP) phases during long time exposure at a high temperature[11,12]. Juraj Belan[13] reported that TCP phases are usually plate-like or needle-like and will reduce rupture strength and ductility.

In this work, the microstructural and precipitation evolution in the nickel-based alloys with different W addition during long-term exposure at 700/750 °C high temperature and the influence on the mechanical properties of the alloys are investigated. The structure and composition of the various phases in alloys are determined, and the role of W is discussed in terms of the formation of precipitates present in the alloy.

2. Experimental procedure

Alloy elements Ni, Co and W with a purity of at least 99.9 wt% as well as Mo-Cr solid solution were molten using a vacuum induction furnace.The new testing alloy was smelted into an ingot by 25kg, and then forged into round bar with 16 mm diameter. The chemical compositions of the new designed alloys are given in Table 1.

Table 1. Chemical compositions of the alloy (wt. %)

Element	C	Cr	Al	Ti	Co	Mo	W	Ni
Alloy1	0.042	19.31	1.45	3.02	13.74	3.53	3.95	Bal.
Alloy2	0.044	19.40	1.38	2.97	13.46	3.56	7.91	Bal.

The as-processed samples were subjected to a standard heat treatment process, which is composed of (1) soaking at 1080 °C for 4 h and oil cooling (OC), (2) soaking at 845 °C for 24 h and then air cooling to room temperature (AC) , (3) aging at 760 °C for 16 h and then air cooling to room temperature (AC). The as-treated samples were subsequently aged at different temperature and time in muffle furnace, 700°C for 1000h, 3000 h, 5000h and 10000h, and 750°C for 3000h and 5000h.

The impact properties after standard heat treatment and long-term exposure were obtained by Charpy V-notch impactor at room temperature. The specimens were divided into two groups and then testing results were averaged. Scanning electron microscope (SEM) was applied to observe the microstructures; Energy dispersive spectrometry (EDS) was applied to analyze the chemical compositions of the precipitates; small-angle X-Ray diffraction (XRD) method was adopted to identify the type of precipitates; the chemical phase analysis method was used to qualitatively and quantitatively analyze the evolution of carbides and TCP phase during long-term exposure. The

transmission electron microscopy (TEM) observations were performed using a JEM-2100F high resolution electron microscope at the operating voltage of 200 kV.

For SEM observation, the experimental samples were mechanically ground and polished consecutively, and then etched with a solution containing 200 ml hydrochloric acid, 200 ml ethyl alcohol and 10g copper dichloride. The method of extraction was used to extract the carbides and TCP with a solution consist of 10 (g/L) ammonium sulfate and 10 (g/L) aqueous citric acid, and the extraction current density was 0.03 A/cm2 at a temperature range of -15 to 20 °C. Before the TEM analysis, foils with a thickness of 50 um obtained by hand grinding were electro-polished at -30 °C and 55-65mA, and the electrolyte was composed of 8% perchloric acid in ethanol

3. Results and discussion

3.1 thermo-calc dynamics calculation

Thermo-calc dynamic calculation software was usually performed to predict the phase formation and stability of alloys [14]. The calculated results of the tentative alloys with different contents of W are shown in Fig.s 1 and 2. Fig. 1(a) shows all the predicted equilibrium phases and their mass fractions in alloy1 which contains 4% W at a temperature range of 500 to 1500 °C. Only the liquid phase forms at 1380 °C (above the liquidus). The γ- Matrix, Mu(u)phase, γ′ phase and $M_{23}C_6$ carbide have been separated out in turn with decreasing temperature and their mass fractions are changing with temperature. The calculated precipitation temperature of u phase, γ′ phase and $M_{23}C_6$ phase are 1130, 1010 and 920 °C, respectively. Fig. 1 (b) shows all the predicted equilibrium phases and their mass fractions in alloy 2, which contains 8% W. One can see there are γ- Matrix, u phase, γ′ phase, σ phase, R phase and $M_{23}C_6$ carbide. And the precipitation temperature of σ phase and R phase are 725 and 580 °C, respectively.

Fig. 2(a) and (b) show the change of predicted equilibrium phases and their mass fractions in the alloys with different W contents at 700 and 750 °C, respectively. One can see the content of u phase increases with the increase of W content and decreases with the increase of temperature. SIGMA phase begins to precipitate when the W content reaches 7.8% and 8.3% at 700 °C and 750 °C, respectively.

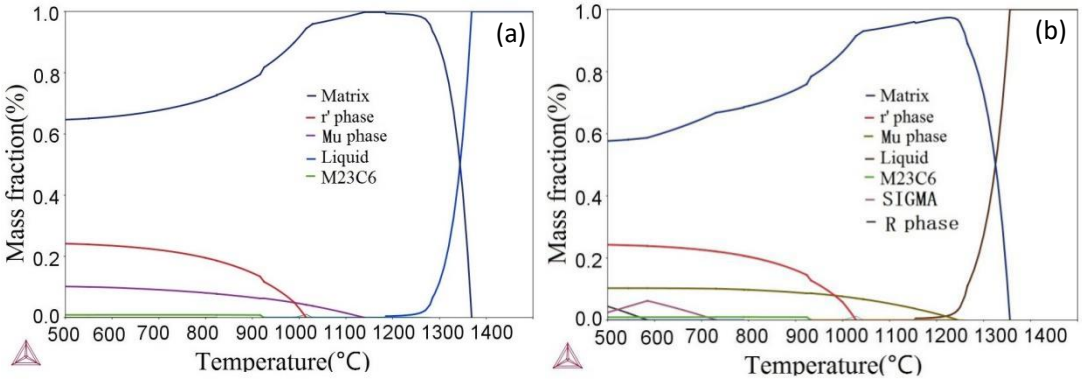

Fig.1. Calculated phase fraction as a function of temperature diagrams for (a) Alloy1; (b) Alloy2;

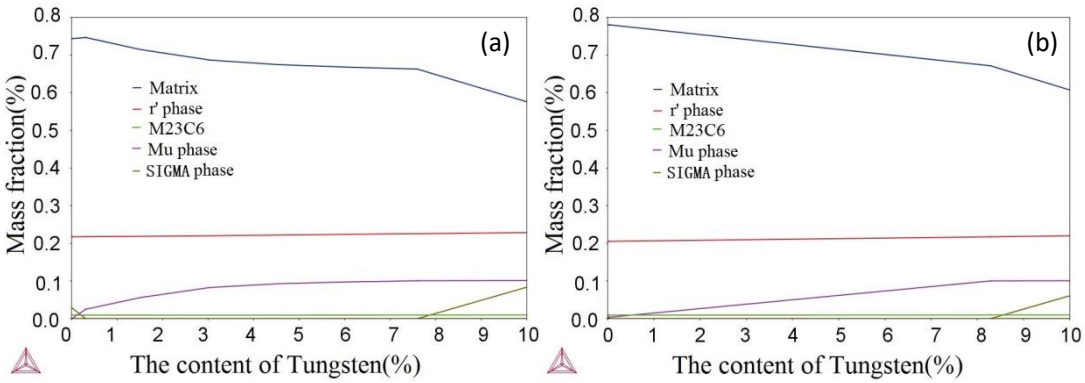

Fig.2. Calculated phase fraction as a function of W content at (a) 700 °C; (b) 750 °C;

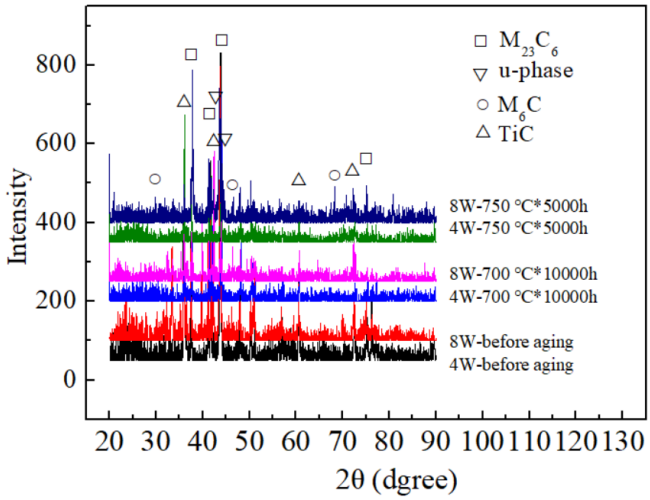

Fig.3. Precipitates detected by XRD;

The XRD results of the alloys with different W content after long-term exposure at 700 and 750 °C are presented in Fig. 3. Only γ′ phase, MC and $M_{23}C_6$ carbides were detected in alloy1 after exposure at 700 and 750 °C. Except γ′ phase, MC and $M_{23}C_6$, M_6C was detected in alloy2 before and after long-term exposure, meanwhile, u phase was found after exposure at 750 °C for 3000h and 5000 h. SIGMA and R phase were not detected in the present work based on method of chemical phase analysis.

Computational thermodynamics verified experimental observations of the formation of γ′, MC, $M_{23}C_6$ and u phase, but amount of MC is very little and it is not show in XRD results. M_6C is an unstable phase. It has been reported that M_6C is a mesophase of u phase [15]. So it cannot exist in the calculation results of equilibrium phase.

3.2 microstructure evolution during exposure

The SEM morphologies of the evolution of microstructure of alloy1 and alloy2 exposed for 0, 5000 and 10000 h at 700 °C are shown in Fig. 3. Both in alloy1 and alloy2, granular Ti-rich MC phase with big size is distributed random inner on the grain boundaries and maintained stability during exposure, as marked by arrow. Most Cr-rich $M_{23}C_6$ particles discontinuously distributed on grain boundaries before exposure and then transformed into continuously distribution after

exposure for 10000 h. Except MC and $M_{23}C_6$ carbides, some W-rich micro-scale round white particles are found in alloy 2 and identified as M_6C phase by XRD, as the arrow marked, M_6C particles are arranged in array inner the grain.

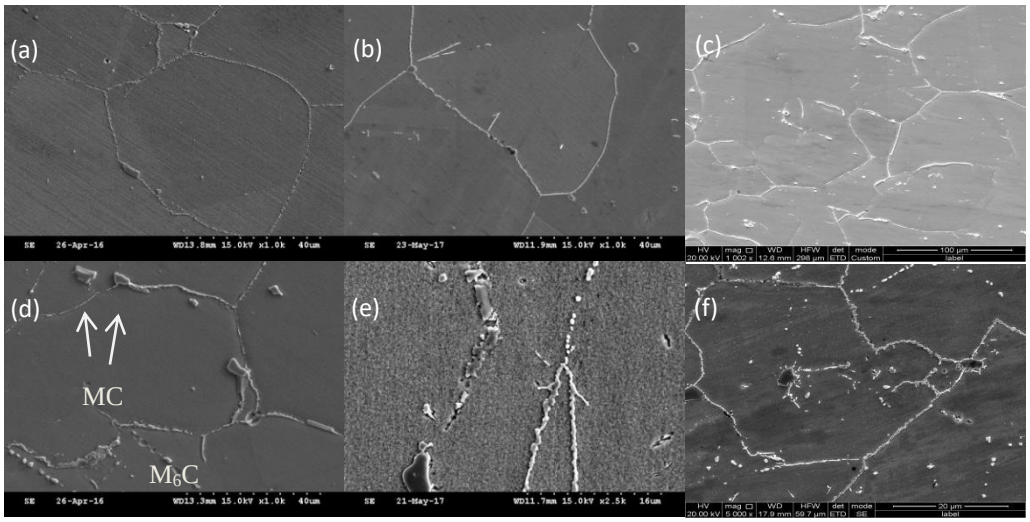

Fig.4 SEM morphologies showing microstructure evolution of alloy 1 after exposure at 700 °C for (a) 0h,(b) 5000h, (c) 10000 h; of alloy 2 for (d) 0,(e) 5000, (f), 10000 h.

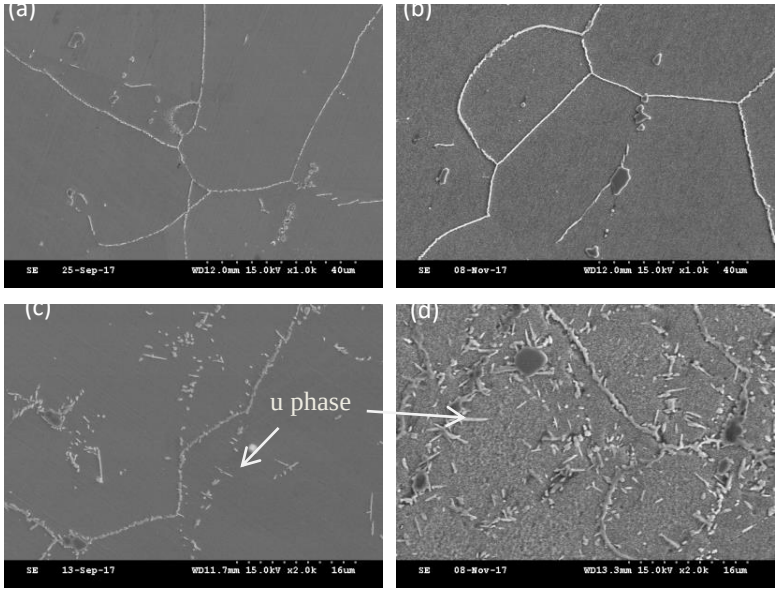

Fig.5 SEM morphologies of alloy 1 after exposure at 750 °C for (a) 3000h, (b) 10000h; of alloy 2 for (c) 3000,(d) 10000 h

The microstructure of the alloy after exposure for 3000h and 5000h at 750 °C obtained by SEM is showed in fig.5. Both in alloy1 and alloy2, the size, amount and morphologies of MC carbides have no remarkable change after 5000 h exposure; the amount of $M_{23}C_6$ carbides on the grain boundary increased obviously with increasing exposure time, meanwhile a large number of $M_{23}C_6$ phase precipitated at grain boundaries, resulting in widening of grain boundaries. A little needle-like precipitates have been observed in alloy 2 after exposure for 3000 h, and the amount

of needle-like precipitation increases significantly with increasing exposure time, as shown in Fig. 5(d). The XRD analysis shows that the needle-like precipitations are u phase, which randomly distributed in grains.

3.3 Evolution of M_6C

When the content of W is high enough, M_6C would precipitate from matrix and the precipitation temperature is higher than that of $M_{23}C_6$ [14-15]. The precipitation evolution during standard heat treatment of alloy 2 is shown in Fig. 6. The W-rich white particles precipitate in the grain after solution treatment at 1080 °C for 4 h, the amount of M_6C increased slightly after pre-exposure at 845 °C for 24 h, meanwhile the $M_{23}C_6$ carbides begin to precipitate on grain boundaries. The morphology and quantity of M_6C carbides keep unchanged during the following aging at 760 °C for 16 h. The chemical compositions of M_6C and $M_{23}C_6$ obtained by EDS are shown in table 2. The total element contents of W and Mo of particle A, B, C is 56.45%, 77.98%, 52.24 %, respectively. The W and Mo content of particle D is 15.75%, but the particle has higher Cr and Ni content than other particles. By comparing the elementary composition of A, B, C, D, and combining their XRD results, it can be inferred that particle A, B, C are M_6C and D particle is $M_{23}C_6$.

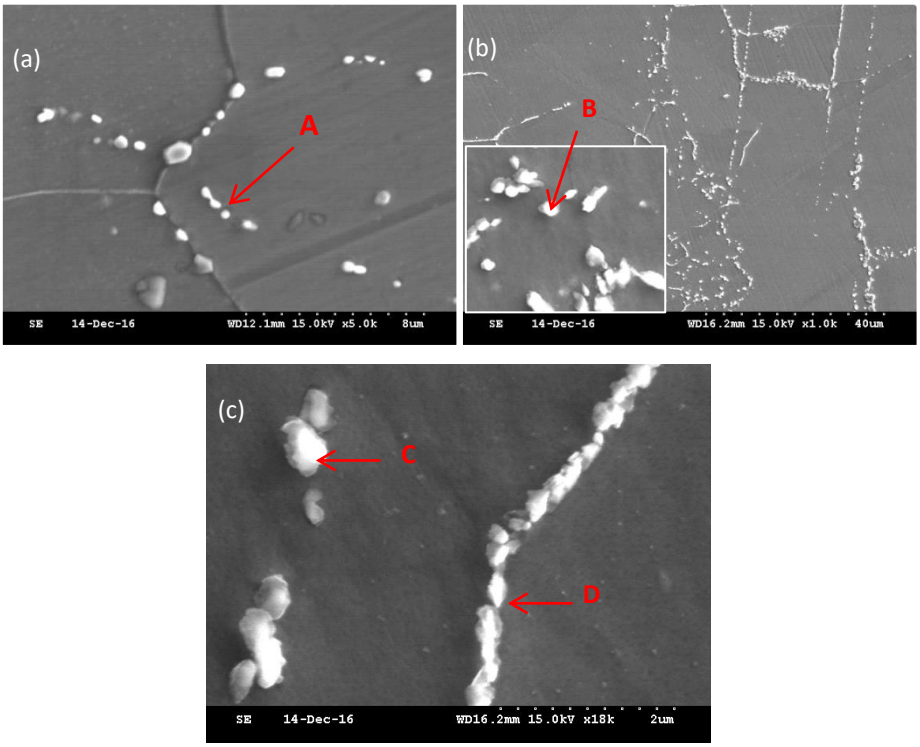

Fig.6 The morphologies of M_6C and $M_{23}C_6$ after different heat-treatment; (a) 1080 °C; (b) 1080 °C + 845 °C; (c) 1080 °C + 845 °C + 760 °C;

Table 2 The element component of different positons with SEM+EDS analysis

Positions	C K	NiL	MoL	TiK	CrK	CoK	W L	AlK	Carbide
A	0.04	18.46	10.75	2.38	14.47	7.93	45.7		M_6C
B	0.02	2.4	17.78	1.28	15.82	2.61	60.2		M_6C
C	0.06	20.47	9.91	2.17	16.31	8.75	42.33		M_6C
D	0.02	**48.77**	3.88	2.82	**18.22**	13.35	**11.87**	1.07	**$M_{23}C_6$**

Research has shown that M_6C phase is an unstable phase and will be transformed into $M_{12}C$ during long-term exposure at high temperature [15]. M_6C and $M_{12}C$ have the same composition and crystal structure (FCC), the difference of them was the $M_{12}C$ has a smaller lattice constant than M_6C, the lattice constant of M_6C is about 1.101 nm and $M_{12}C$ is about 1.085 nm. The lattice constant of M_6C in alloy 2 detected by chemical phase analysis and XRD is at the range of 1.104 to 1.106 nm. Bright-field image and the select area diffraction pattern (SADP) of alloy 2 after exposure at 750°C for 5000 h obtained by JEOL-2100F TEM are showed in Fig.7. The Fig. shows a particle suspected to be M_6C phase with a size of 500 nm is surrounded by some spherical γ′ phase, and the SADP of the particle marked with a red circle show that the particle has FCC structure and the lattice constant is 1.086 nm with a zone axis [110]. So the particle could be identified as $M_{12}C$.

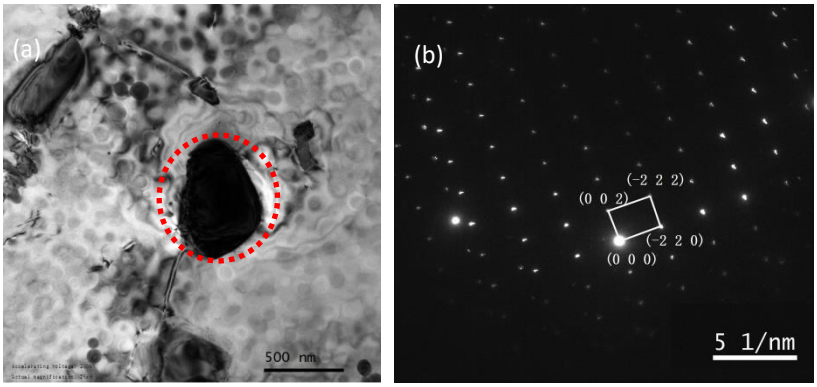

Fig.7 The $M_{12}C$ precipitation after exposure at 750 °C for 5000 h；(a) Bright field image of $M_{12}C$ carbide；(b) SAD pattern of (a)；

3.4 Evolution of u phase

The u phase belongs to topological close-packed phase (TCP) and rhombohedral crystal structure. It is shown that u phase and M_6C have similar close-packed arrangement, and so the alloy which has M_6C precipitate tends to have u phase. When the total amount of molybdenum and tungsten in the alloy exceeds 10%, it is easy to precipitate u phase [16,17].

The u phase in alloy 2 was analyzed by means of SEM, TEM, XRD and chemical phase analysis. Fig.7 shows the SEM images of alloy2 after exposure different time at 750 °C. After exposure for 1000 hours, $M_{23}C_6$ and M_6C precipitated from matrix, and only very little needle-like

u phase precipitated around MC carbide particle, as Fig. 8 (a) shows. The amount of needle-like u phase increased slightly after 3000 h exposure, however, a large amount of u phase precipitated after 5000 h exposure.

The element compositions of granular M_6C precipitation and needle-like u phase detected by EDS at different exposure time are listed in Table.3. In Fig.9 (a), the granular precipitations (position "1") have higher W content than that of needle-like precipitation (position "2"), the needle-like precipitation have lower Ni and Co content than granular precipitation. The chemical phase analysis shows that the granular precipitation is M_6C phase and the acicular precipitation is u phase, therefore, it can be concluded that M_6C has higher W content and lower Co and Ni content than u phase.

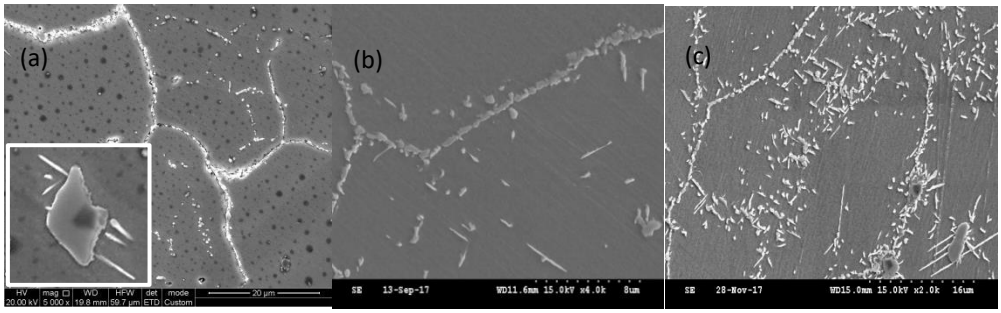

Fig.8 The precipitates in alloy 2 after different exposure time at 750°C; (a) 1000 h; (b) 3000 h; (c) 5000 h;

Fig.9 The precipitates of alloy 2 after long-term exposure at 750°C; (a-b) 3000h; (c) 5000h;

Table.3 The element components of different precipitates with SEM+EDS analysis

Positions	C	MoL	TiK	CrK	CoK	NiK	W L	AlK	Carbide
1	0.05	7.31	2.24	17.65	7.87	30.24	34.03	0.62	M_6C
2	0.06	7.26	2.17	15.62	12.38	36.3	26.21	-	μ
3	0.03	6.69	2.16	14.92	12.25	34.11	29.2	0.64	μ
4	0.06	10.2	-	20.79	5.83	21.61	41.5	-	M_6C

A TEM micrograph of a needle-like u phase is shown in Fig. 10 (a). The u phase around 0.1 um wide and 6.5 um length precipitated in the grain . The Fig.6 (b) is a local enlargement of the area in Fig. 6 (a), it could be found that lots of parallel fringes in u phase. The SADP of u phase is shown in Fig. 6 (c). The diffraction spots are stretched along the vertical direction of fringes in u

phase, which means that there are a lot of stacking faults in the u phase[18,19], and the parallel fringes are the morphologies of stacking faults. Fig. 6 (d) shows a stacking fault cross a γ′ particle. Some needle-like u phases precipitate randomly in matrix, as shown in Fig. 6 (e) . Meanwhile, it could be found that some u phases nucleated around M_6C particles and grew outward. Some parallel fringes like stacking faults were observed near u phase but identified as an initial morphology of u phase.

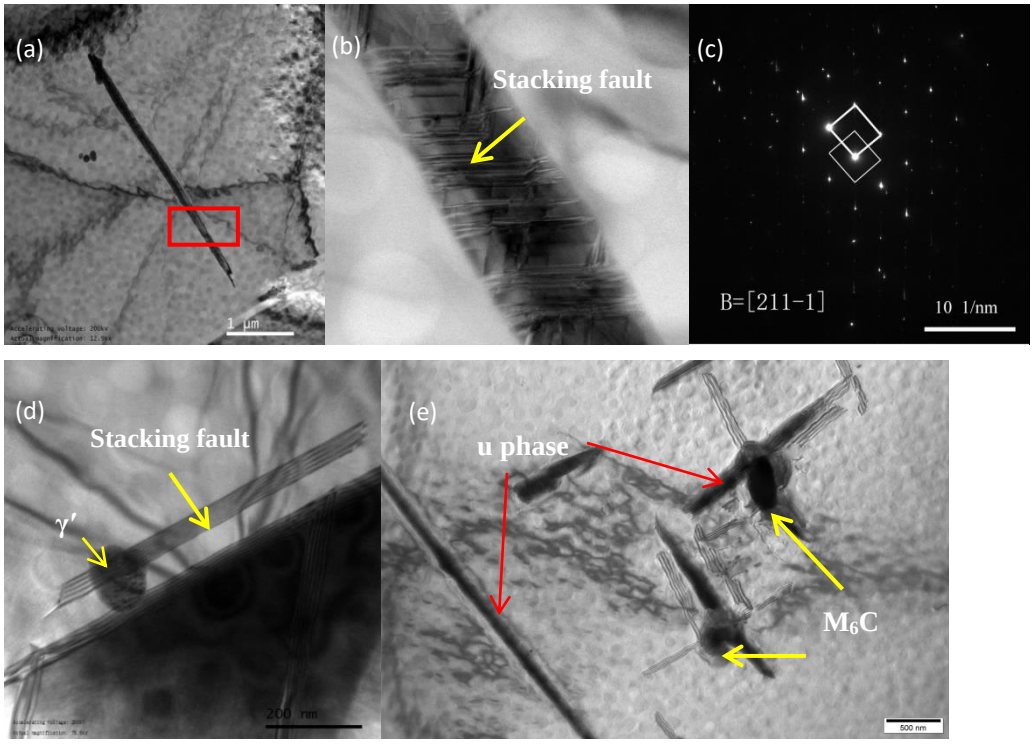

Fig.10 The TEM images of Stacking faults and μ phase in alloy 2 after exposure at 750 °C for 5000h; (a) and (b) the needle-like u phase; (c) SADP of u phase in image (a); (d) and (e) stacking faults and u phase;

Since refractory W and Mo elements have bigger atom size and weight, their diffusion rates are very low, therefore the segregation of W and Mo could not be eliminated completely after solution heat treatment. As a result, the content of refractory elements in some areas are much higher than in other regions, which leads to the formation of r- matrix and makes these areas more easily reach super saturation state and produceM_6C and TCP phase precipitates [20]. Thermodynamic calculations show that only u phase can precipitate from r-matrix at 700 and 750 °C，but M_6C can't. Some reports have shown that M_6C is an unstable phase and is a mesophase of u phase, for it has a similar atoms arrangement structure with u phase and can translate into u phase at specific thermodynamic conditions [21]. It can be found that M_6C transforms into $M_{12}C$ during 5000 h exposure at 750 °C, M_6C transforms into u phase has not been observed during exposure. That means the formation of u phase needs higher thermodynamic driving force than M_6C, and will probably precipitate at higher temperature.

Because of the large particle size and no strengthening effect, the acicular precipitates will reduce the room temperature plasticity and toughness [22]. The change of toughness with

exposure temperature is shown in Fig.11. Exposure at 700 °C, the impact absorbing energy of two alloys decreased obviously at the initial 1000 h exposure, and the decrease trend slowed down during 1000 to 5000 h, and then kept unchanged after 5000h exposure. The impact absorbing energy of two alloys decreased obviously at the initial 3000 h exposure, and then kept unchanged after 3000h exposure at 750°C. The reason of Alloy 2 has lower impact absorbing energy than alloy 1 is that the higher W addition in alloy 2 has decreased the movement of dislocation and resulted in more stress concentration during deformation. So, the crack can spread more easily. The main precipitation period of u phase at 750 °C is during the exposure from 3000 to 5000 h, but the impact absorbing energy was unchanged during this exposure time. The result can be obtained that u phase has no obvious effect on the impact absorbing energy of alloy 2. The possible reason is that u phase mainly precipitates in grains, but the fracture of alloy is mainly inter-granular.

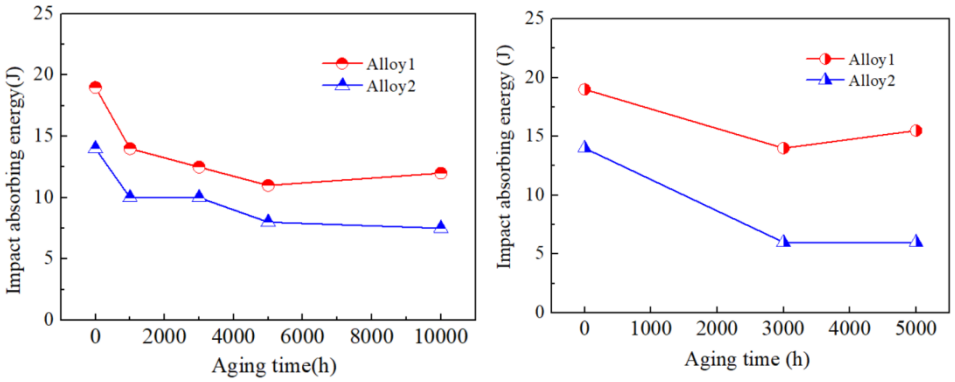

Fig.11 The impact absorbing energy after long-term exposure; (a) 700 °C; (b) 750 °C;

The mass fractions of MC, M_6C and u phase in alloy 2 after long time exposure at 700 and 750 °C are shown in table.4. The MC, M_6C and u phase have similar structure and cannot be separated by chemical phase analysis, the values of table 3 are the sum of mass percentage of them. During 700 °C exposure, the mass fraction of M_6C and MC increased from 0.227 to 0.353 after 1000 h exposure, and reached 0.701 after exposure for 3000 h, then kept unchanged. MC is a stale phase and keep unchanged during exposure, therefore, it can be concluded that the increment content of precipitated phase is M_6C. The mass fraction of the precipitated phases increased observably from 0.227 to 2.058 after 3000 h exposure at 750 °C, reached to 2.894 after 5000 h exposure. From Fig. 7, it can be found that only MC, M_6C and very small amount of u phase precipitated after 3000 h exposure, meanwhile, the content of MC phase does not change with increasing exposure time. So it means M_6C gives the main contribution to the mass fraction of precipitaes within 3000 h exposure and u phase has given its part of contribution mainly in the time range of 3000 to 5000 h.

Table.4 The mass fraction of MC+M_6C+u precipitations of alloy2 after exposure (wt.%)

Exposure time(h)	700	Precipitation	750	Precipitation
0	0.227	MC+ M_6C	0.227	MC+ M_6C
1000	0.353	MC+ M_6C	-	-
3000	0.701	MC+ M_6C	2.058	MC+ M_6C+a little u phase
5000	0.713	MC+ M_6C	2.894	MC+ M_6C+u
10000	0.67	MC+ M_6C	-	-

3 Conclusion

The following conclusions can be drawn from experimental observation and thermodynamic calculation:

(1) Phase equilibria of the Ni-Co-Cr-Mo-W system at the temperature range of 500 °C to 1500 °C have shown the major phases in the alloy include: $M_{23}C_6$, γ′ phase, u phase, MC and M_6C; M_6C and u phase were only observed in the alloy with higher W content.

(2) The M_6C precipitated during solution heat treatment, the amount of which increased with initial 3000 h exposure time, and then kept unchanged, meanwhile, the amount of precipitation at 750 °C is obviously more than that at 700 °C. Part of M_6C transformed to $M_{12}C$ after 5000 h exposure at 750 °C.

(3) Needle-like u phase precipitated after 1000 h exposure at 750°C, the amount of it increased markedly at following exposure time. The main elements of u phase were Ni, W, Co, Cr and Mo.

(4)The impact absorbing energy of the alloy with high W content was low. But u phase has not obvious effect on the impact property during ageing at 750 °C.

Acknowledgments

The authors acknowledge the financial support from the National Key Research and Develop Program, China. (No.2017YFB0305203)

Reference:

1 P.D. Jablonski, J.A. Hawk, C.J. Cowen, P.J. Maziasz. Processing of advanced cast alloys for A-USC steam turbine applications. Jom 64 (2012) 271-279.

2 LIU Zheng-dong, CHENG Shi-chang, TANG Guang-bo , BAO Han-sheng , YANG Gang, GAN Yong. The State-of-the-Art of Steel Technology Used for Chinese Power Plants and Its Future. Iron & Steel (chinese), 2011,46(3),1-5.

3 Fujio Abe, H. Kutsumi, H. Haruyama, H. Okubo. Improvement of oxidation resistance of 9 mass% chromium steel for advanced-ultra supercritical power plant boilers by pre-oxidation treatment Original Research Article. Corrosion Science, Volume 114, Issue 0, 2017, 1-9 .

4 Yuji Fukuda. Development of Advanced Ultra Supercritical Fossil Power Plants in Japan：Materials and High Temperature Corrosion Properties. Materials Science Forum. Vol 696 (2011), 236-241.

5 A.D. Gianfrancesco. Materials for Ultra-Supercritical and Advanced Ultra-Supercritical Power Plants, 13-New Japanese materials for A-USC power plants, Woodhead Publishing, 2017, pp. 449-454.

6 F. Abe. Research and development of heat-resistant materials for advanced USC power plants with steam temperatures of 700 °C and above, Engineering 1(2015) 211-224.

7 Takeshi Kuramochi. Review of energy and climate policy developments in Japan before and after Fukushima. Renewable and Sustainable Energy Reviews, 2015, 43: 1320-1332.

8 Materials Science and Engineering for super alloys (Volume one). Guo Jianting. Science press (Chinese),2008.

9 Fujio Abe. Research and Development of Heat-Resistant Materials for Advanced USC Power Plants with Steam Temperatures of 700 °C and Above. Engineering 2015, 1(2): 211–224.

10 Liang Zheng, Chengbo Xiao, Guoqing Zhang. Brittle fracture of gas turbine blade caused by the formation of primary b-NiAl phase in Ni-base superalloy. Engineering Failure Analysis, 26 (2012) 318–324.

11 R. Popp , S. Haas , F. Scherm , A. Redermeier , E. Povoden-Karadeniz , T. G€ohler , U. Glatzel. Determination of solubility limits of refractory elements in TCP phases of the Ni-Mo-Cr ternary system using diffusion multiples. Journal of Alloys and Compounds, 788 (2019) 67-74.

12 I.S. Kim, B.G.Choi, H.U.Hong, J.Do, C.Y.Jo. Influence of thermal exposure on the microstructural evolution and mechanical properties of a wrought Ni-base superalloy. Materials Science & Engineering A, 593(2014)55–63.

13 Juraj Belan. GCP and TCP phases presented in nickel-base superalloys. Materials Today: Proceedings 3, (2016) 936 – 941.

14 Chan-Jin Park, Myung-Kyu Ahn, Hyuk-Sang Kwon. Influences of Mo substitution by W on the precipitation kinetics of secondary phases and the associated localized corrosion and embrittlement in 29% Cr ferritic stainless steels. Materials Science and Engineering A, 418 (2006) 211–217.

15 Wang Lu , Yang Gang, Liu Zhengdong, Wang Li, Ma Longteng, Yang Zhiqiang. Effects of Long-term Aging on Microstructure and Mechanical Properties of a Nickel-base Alloy. Rare Metal Materials and Engineering(Chinese). 2018,(47)3,961-967.

16 G.B. Viswanathan, R. Shi,a A. Genc, V.A. Vorontsov, L. Kovarik, C.M.F. Rae, M.J. Mills. Segregation at stacking faults within the γ′ phase of two Ni-base superalloys following intermediate temperature creep. Scripta Materialia, 94 (2015) 5 – 8.

17. E. Fleischmann, M.K. Miller, E. Affeldt, U. Glatzel. Quantitative experimental determination of the solid solution hardening potential of rhenium, tungsten and molybdenum in single-crystal nickel-based superalloys, Acta Mater. 87 (2015) 350-356.

18 Huifang Li, FeiYea, JieZhao, Tieshan Cao, Fanghong Xu, Qingshuang Xua,Yan Wang, Congqian Cheng, Xiaohua Min. Grain boundary migration-induced directional coarsening of the γ′ phase in advanced ultra-supercritical superalloy. Materials Science and Engineering: A, 2018,714(0), 172-178.

19 Y. I.dell , L.E. Levine, A.J. Allen, F. ZHANG, C.E. Campbell, G.B. Olson, J. GONG, D.R. Snyder, H.Z. Deutchman. Unexpected δ-Phase Formation in Additive-Manufactured Ni-Based Superalloy. JOM, Vol. 68, No. 3, 2016.DOI: 10.1007/s11837-015-1772-2

20 Z. Chen, J. W. Brooks , M. H. Loretto. Precipitation in Incoloy alloy 909. Materials Science and Technology, 9:8, 647-653, DOI: 10.1179/mst.1993.9.8.647.

21 A. Kermanpur, N. Varahraam, E. Engilehei, M. Mohammadzadeh, and P. Davami. Directional solidification of Ni base superalloy IN738LC to improve creep properties. Materials Science and Technology. May 2000 ,Vol. 16.579-586

22 R.C. REED, M.P. JACKSON, and Y.S. NA. Characterization and Modeling of the Precipitation of the Sigma Phase in UDIMET 720 and UDIMET 720LI. Metallurgical and Materials Transactions A, Volume 30A, March 1999-521.